



ELSEVIER

Available online at www.sciencedirect.com

 ScienceDirect

Proceedings of the Combustion Institute 33 (2011) 2143–2152

Proceedings
of the
Combustion
Institute

www.elsevier.com/locate/proci

Direct numerical simulations and analysis of three-dimensional *n*-heptane spray flames in a model swirl combustor

K. Luo^{a,*}, H. Pitsch^b, M.G. Pai^b, O. Desjardins^c

^a State Key Laboratory of Clean Energy Utilization, Zhejiang University, Hangzhou 310027, PR China

^b Center for Turbulence Research, Stanford University, CA 94305, USA

^c Department of Mechanical Engineering, University of Colorado at Boulder, CO 80309, USA

Available online 17 September 2010

Abstract

Three-dimensional *n*-heptane spray flames in a swirl combustor are investigated by means of direct numerical simulation (DNS) to provide insight into realistic spray evaporation and combustion as well as relevant modeling issues. The variable-density, low-Mach number Navier–Stokes equations are solved using a fully conservative and kinetic energy conserving finite difference scheme in cylindrical coordinates. Dispersed droplets are tracked in a Lagrangian framework. Droplet evaporation is described by an equilibrium model. Gas combustion is represented using an adaptive one-step irreversible reaction. Two different cases are studied: a lean case that resembles a lean direct injection combustion, and a rich case that represents the primary combustion region of a rich-burn/quick-quench/lean-burn combustor. The results suggest that premixed combustion contribute more than 70% to the total heat release rate, although diffusion flame have volumetrically a higher contribution. The conditional mean scalar dissipation rate is shown to be strongly influenced, especially in the rich case. The conditional mean evaporation rate increases almost linearly with mixture fraction in the lean case, but shows a more complex behavior in the rich case. The probability density functions (PDF) of mixture fraction in spray combustion are shown to be quite complex. To model this behavior, the formulation of the PDF in a transformed mixture fraction space is proposed and demonstrated to predict the DNS data reasonably well.

© 2010 The Combustion Institute. Published by Elsevier Inc. All rights reserved.

Keywords: Direct numerical simulation; Spray evaporation; Combustion; Swirling flames; Conditional moment

1. Introduction

Spray combustion is encountered in a variety of engineering applications that include gas-turbine aircraft engines and internal combustion engines. The concurrent processes of liquid phase

dynamics, turbulence, as well as combustion, strongly interact with each other making experimental measurement or high-fidelity simulation of spray combustion very challenging.

Direct numerical simulations (DNS) of spray combustion are becoming commonplace and can potentially resolve all instantaneous scales of chemical reactions and turbulent hydrodynamics. Thus, DNS plays an important role in studying spray combustion. Recently, some DNS studies

* Corresponding author. Fax: +86 57187951764.

E-mail address: zjulk@zju.edu.cn (K. Luo).

of spray combustion have been performed [1–4]. However, these studies are limited to simple two-dimensional configurations. Turbulent flows and spray flames are essentially three-dimensional, and realistic spray combustion often occurs in complex configurations. Furthermore, the tight coupling between evaporation and combustion needs to be addressed. There is thus a pressing need to study three-dimensional spray combustion in moderately complex configurations.

To gain a better understanding of spray combustion in a realistic configuration, DNS of *n*-heptane spray flames in a model swirl combustor has been performed. The parameters of the simulations are chosen to approach realistic spray combustion in a gas-turbine combustor within the limits of current computational capabilities. Analysis of the spray flames, conditional means, and PDFs of mixture fraction are reported. Potential insights into spray combustion and relevant modeling issues are discussed.

2. Mathematical models

In the present simulations, the variable-density, low-Mach number Navier–Stokes equations for the gas phase are solved in an Eulerian framework, whereas the governing equations for the dispersed phase are described using a Lagrangian formulation. Three scalar transport equations corresponding to the mass fractions of fuel (*F*), oxidizer (*O*), and products (*P*) are solved based on an adaptive one-step combustion model that can correctly reproduce the burning rate for both lean and rich mixtures [5]. A transport equation for gas temperature is also solved (neglecting the viscous heating term):

$$c_p \frac{\partial \rho T}{\partial t} + c_p \frac{\partial \rho T u_j}{\partial x_j} = \frac{\partial}{\partial x_j} \left(\lambda \frac{\partial T}{\partial x_j} \right) + \dot{\omega}_T + \dot{S}_T, \quad (1)$$

where \dot{S}_T is the energy exchange rate with the droplets, and $\dot{\omega}_T$ is the rate of heat release by combustion. The heat capacity c_p and the thermal conductivity λ are kept constant. Likewise, the Lewis numbers of all species are assumed to be unity.

Dispersed particles evolve according to the BBO equation. However, owing to the high density ratio ($\rho_L/\rho \gg 1$) between liquid *n*-heptane droplets and air, only dominant drag force and gravity are considered, whereas Basset history, added mass effects and other unsteady drag effects are neglected [6]. Collisions and coalescence are also neglected, as the volumetric loading of droplets is small. Considering both complexity and accuracy, an equilibrium, infinite thermal conductivity model for droplet evaporation [7] is used. The droplets are treated as point sources of mass, momentum, and energy to the gas phase which is valid for a spray with droplet diameters smaller

than the smallest gas-phase length scale. Detailed two-phase governing equations, verification, and validation of droplet evaporation and gas combustion models can be found in a previous study [8].

3. Numerical details

3.1. Flow configuration and grid system

The flow geometry of the model combustor is shown in Fig. 1. The central swirling air of temperature 500 K is injected through a pipe of inner diameter $D_{\text{cin}} = 3.75$ mm with a mean axial velocity $U_{\text{inj}} = 4.5$ m/s and a mean swirl velocity $W_{\text{inj}} = 4.5$ m/s. The secondary swirling air of temperature 500 K is injected through an annular pipe of inner diameter $D_{\text{sin}} = 5$ mm and outer diameter $D_{\text{cout}} = 10$ mm with the same mean axial and swirl velocities as those of the central one. This corresponds to a geometric swirl number $S = 1.0$. The combustion chamber is 40 mm wide and 60 mm long, and the outside injection pipe is 10 mm long. The flow Reynolds number based on the mean axial velocity and outer diameter of the pipe is about 3000. The spray is assumed to have been fully atomized, and the resulting *n*-heptane droplets are issued from the tip of the wall regions between the central and the annular pipes with a temperature of 300 K. When the droplets are issued, they are assumed to be in dynamical equilibrium with and have the same velocities as the carrier air. This leads to a spray cone angle of 90° and droplets in the low Weber number limit. Thus, secondary break-up of droplets is unimportant and therefore not considered in the present simulations. A log-normal droplet size distribution with mean diameter $10 \mu\text{m}$, maximum diameter $20 \mu\text{m}$, and minimum diameter $1 \mu\text{m}$ is used to characterize the issued droplets.

In DNS of spray combustion, there are strict requirements to the grid resolution. On the one hand, the grid size has to be small enough to resolve both the Kolmogorov length scale and the reaction zone thickness of the flame. On the other hand, the grid size has to be around 10 times

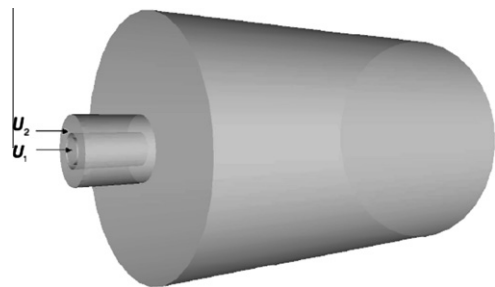


Fig. 1. Geometry of the model combustor.

larger than the droplet size to get correct droplet evaporation dynamics if the point-source assumption of droplet is used, as demonstrated in a previous study [8]. To determine the grid resolution, grid-dependence studies have been performed. The grid resolution with 768 nodes along the axial direction, 384 nodes along the radial direction, and 256 nodes along the swirling direction resulting in about 75 million mesh points is chosen in the present study. A non-uniform grid is employed with finer grids used in the recirculation, strong shear and near-wall regions. The DNS results demonstrate that the reaction zone is typically resolved by 8–10 grid points which confirms the adequacy of the grid [9] for this test case.

3.2. Boundary conditions and numerical algorithm

No-slip wall boundary conditions are used in the radial direction. The downstream convective outflow condition allows for a smooth exit of all structures without perturbing the rest of the flow. To generate turbulent inflow conditions for the swirling air jets, separate DNS of pipe flows are conducted, and read in as the inflow boundary conditions. At first, hot air with temperature 1500 K is injected to accelerate the evaporation and trigger the combustion. Then the temperature is reduced to 500 K. Datasets for post-processing are recorded after the flames become statistically steady.

Lean direct injection (LDI) and rich-burn/quick-quench/lean-burn (RQL) are two of the prominent low-emissions concepts for aircraft engines. Both use liquid fuel injection, but LDI operates the primary combustion region lean, hence, adequate flame stabilization has to be ensured; RQL is rich in the primary zone with a transition to lean combustion by rapid mixing with secondary air downstream. Hence, both concepts avoid stoichiometric combustion as much as possible, but flame stabilization and combustion in the main heat release region are entirely different. To simulate both of these cases, the droplet mass flow rate is adjusted to provide a global equivalence ratio of 0.7 (lean) and 2.1 (rich), respectively. The central and secondary jets have the same swirl direction. Among the various parameters that influence spray combustion, we focus only on the equivalence ratio in the present study. Table 1 displays the comparison of major parameters between a typical gas-turbine combustor, evaluated from the LES of a Pratt and Whitney 6000 combustor [10,11], and the model combustor in this study. The main difference is the flow Reynolds number, droplet Stokes number and droplet Weber number, all of which are chosen within the limitations of current point-particle DNS approaches for spray combustion.

The Navier–Stokes equations are discretized in a cylindrical coordinate using a second-order

Table 1

Comparison of major parameters between realistic gas-turbine combustor, evaluated from the LES of a Pratt and Whitney 6000 combustor [10,11], and the model combustor in the present DNS.

Parameter	Turbine	Model
Spray cone angle	90°	90°
Density ratio	O(10 ³)	O(10 ³)
Swirl number	1.0	1.0
Damköhler number	O(50)	O(50)
Karlovitz number	O(0.1)	O(0.1)
Reynolds number	O(10 ⁶)	O(10 ³)
Stokes number	2.5–10	0.1–0.4
Weber number	O(50)	O(0.1)

kinetic energy conserving finite difference scheme in space and a second-order semi-implicit scheme in time [12]. Governing equations of droplets are advanced first, followed by the scalar and momentum equations. The velocities are then corrected by solving a Poisson equation so that they satisfy mass continuity. The equations for species mass fractions and for the temperature are rendered especially stiff because of the chemical source terms. As a result, a fully implicit treatment of the chemical source terms is required and has been implemented for an accurate integration. The spray is described with a Lagrangian solver that uses a second-order Runge–Kutta time integration for droplets equations. The information from the gas phase is interpolated at the droplet positions using a tri-linear interpolation. Once the droplet diameter falls below 0.5 μm , it is removed from the calculation, and the remaining mass, momentum, and energy are transferred to the gas phase.

4. Results and discussions

4.1. Premixed and diffusion flame structures

Previous DNS studies have shown that spray combustion is composed of both premixed flames and diffusion flames [1–3]. To visualize the flame structures for the present swirl spray combustion configuration, the normalized flame index [2] is used. This quantity is plotted for the reactive regions of the lean case in Fig. 2. The figure shows first of all that the structure of the spray flame is quite complicated. There are not only isolated diffusion flame and premixed flame regions, but mostly composite structures. For instance, as indicated in the figure, there are pockets of diffusion flames enclosed by pockets of premixed flames, pockets of premixed flames enclosed by diffusion flames, and premixed flame bands connecting diffusion flames. In addition, there are local non-burning pockets within burning flames. Interestingly, the coupled structures often consist of thick rich premixed heat release regions with very thin

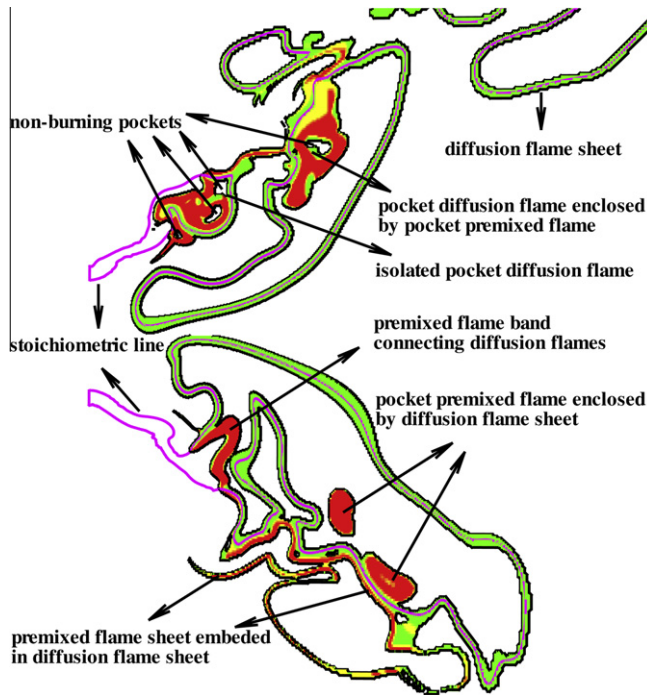


Fig. 2. Instantaneous spray flame structures for the lean case (purple: stoichiometric mixture fraction iso-line; green: diffusion flames; red: premixed flames).

diffusion flame layers. As expected, diffusion flames mostly occur around stoichiometric conditions. In contrast, premixed combustion is typically found in the rich regions.

It is interesting also to note that the flame is lifted off the nozzle. Hence, non-reactive mixing occurs in the early dense region of the spray development, which leads to a rich region surrounded by stoichiometric mixture. The rich region leads into a rich premixed combustion zone with thin diffusion flame layers attached at the points where stoichiometric mixture meets the rich combustion region. All these complex structures are related to the dynamics of the swirling flow and turbulent mixing, and bring significant challenges for spray combustion modeling. Corresponding to Fig. 2, Fig. 3 shows the instantaneous distributions of temperature and fuel mass fraction that further confirm the above observations.

Figure 4 presents instantaneous droplet location and contours of flame index for the region close to the spray injection for both cases. For the lean case, most droplets, acting as vapor sources, are separate from the flame front. Combustion starts only after the spray is sufficiently diluted due to evaporation and entrainment of the surrounding air. Also for this instant, the main flame stabilization appears as a combination of a rich premixed combustion region central to the jet with surrounding diffusion flame layers.

Both the spray flame structures and the droplet combustion mode substantially change when the global equivalence ratio is increased to 2.1. The droplets have a longer trajectory, but the flame becomes more compact. Here, the central recirculation zone brings rich evaporated fuel vapor back towards the nozzle and a rich premixed flame establishes along the inner surface of the spray cone. Also the outer recirculation regions return rich evaporated fuel towards the bulk head of the combustor. Close to the bulk head, this rich mixture mixes with the outer air inlet and establishes a diffusion flame that surrounds the spray cone. Just as for the lean case, a non-reacting stoichiometric surface surrounds the dense spray close to the nozzle. In the outer high shear region, this surface remains non-reactive until all the droplets are evaporated. On the inside of the spray cone, the inner recirculation region leads to good mixing, longer residence times, and recirculated rich hot combustion products. This rich mixture mixes with the centrally injected air and establishes a very robust diffusion flame in the center, which lights the rich premixed flame downstream. This leads to a stabilization mechanism that is clearly different from the lean case. Furthermore, from these observations it can also be speculated that for both the rich and the lean cases, droplet evaporation is mainly driven by the rich premixed combustion regions.

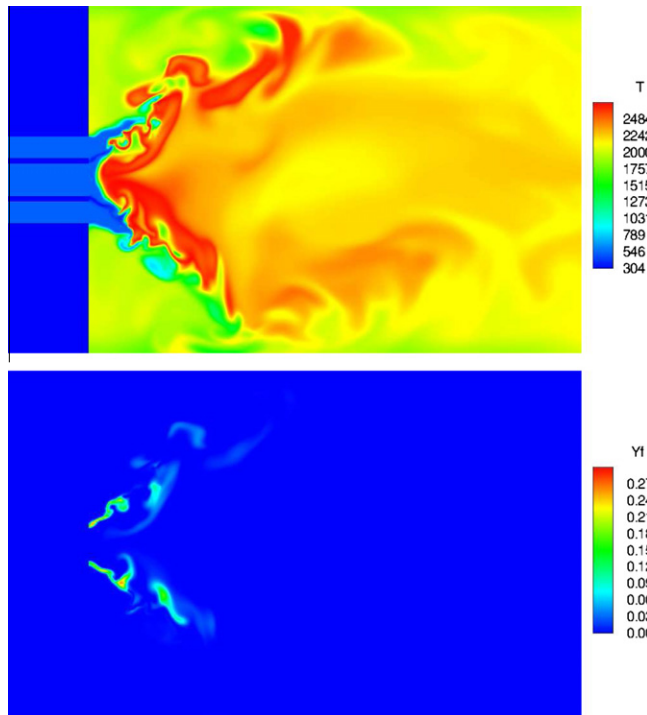


Fig. 3. Instantaneous distribution of temperature and fuel mass fraction for the lean case (top: temperature; bottom: fuel mass fraction).

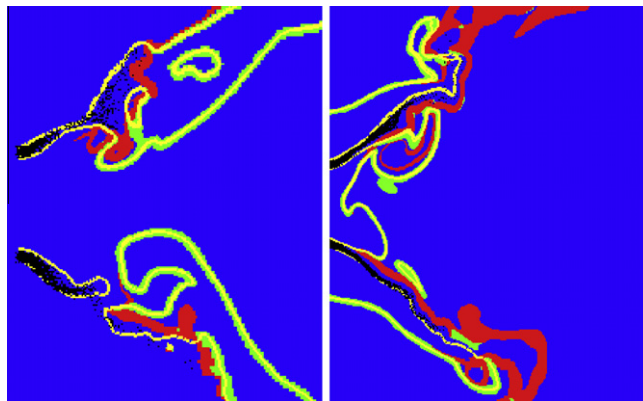


Fig. 4. Instantaneous droplets superimposed on contour of flame index for the lean (left) and rich (right) cases (red color denotes premixed flame, green color denotes diffusion flame, and black points are droplets).

To differentiate the roles of premixed and diffusion flames, the conditional mean evaporation, total combustion, premixed, and diffusion combustion source terms are computed as planar averages along the x direction:

$$\langle \dot{\omega}_i(x) \rangle = \frac{\int \int \beta_i \dot{\omega}_i dr d\theta}{\int \int dr d\theta}, \quad (2)$$

where $\dot{\omega}_i$ stands for the source terms corresponding to evaporation, total combustion, premixed, and diffusion combustion. β_i is a constant, set to unity for calculating the conditional mean evaporation and total combustion source terms, and equal to the local flame index [2] (1 for local premixed flame and 0 for local diffusion combustion) when calculating the conditional mean premixed or diffusion combustion source term.

Figure 5 presents the distribution of the conditional means along the axial direction. For both the rich and the lean cases, evaporation peaks close to the injection point. For the lean case, the fuel evaporates close to the nozzle followed by a strong premixed combustion peak. Premixed combustion discontinues slightly downstream of the disappearance of liquid fuel. This region is followed by a long diffusion combustion region of relatively low heat release. The rich case is similar, but because more fuel is injected, the evaporation and premixed combustion regions extend further downstream. It is interesting to note here that both premixed and non-premixed combustion extend to approximately the same downstream cross-section. It is surprising to find that premixed combustion contributes more than 70% to the total combustion rate for both lean and rich cases although diffusion combustion appears over a larger region. It is particularly interesting to note that the rich case, which does not show the trailing diffusion combustion region, seems to be even more governed by premixed combustion than the lean case. This finding certainly has important implications for modeling, particularly, since spray combustion is most often treated using purely non-premixed combustion models. It should be noted here that these observations are related to a large degree to the evaporation process and mixing of fuel and air, and further that a kinetic model has been used here that properly represent combustion characteristics in rich mixtures. Therefore, it is expected that similar conclusions would also be found in simulations using multi-step chemical kinetics.

To further investigate the characteristics of premixed flames in spray combustion, scatter plots of Karlovitz number with mixture fraction for premixed flames are shown in Fig. 6. It is found that most premixed combustion in the studied cases occurs in the wrinkled and corrugated

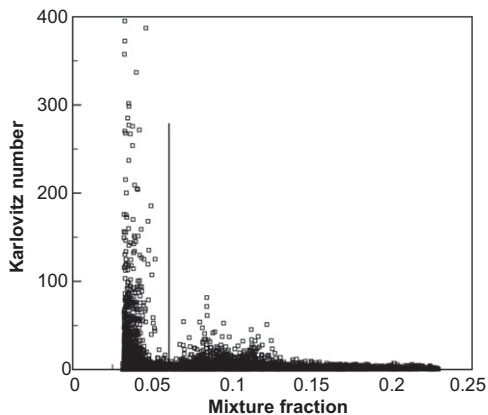


Fig. 6. Scatter plots of Karlovitz number in mixture fraction space for premixed combustion in the lean case (solid line corresponds to the stoichiometric mixture fraction 0.062).

flamelets regime ($Ka < 1$), as well as in the thin reaction zone regimes ($1 < Ka < 100$), which justifies the application of flamelet type models. While this conclusion might be a result of the chosen global parameters of the simulations, it should be noted that the combustion parameters have been chosen to match typical conditions in aircraft engines.

4.2. Conditional mean scalar dissipation rate

Most diffusion combustion models rely on the scalar dissipation rate to describe mixing process between fuel and oxidizer. In flamelet modeling, it is a common practice to assume the shape of the conditional mean scalar dissipation rate to be a function of mixture fraction. However, this assumption may not be applicable to spray combustion, as the mixing process is modified by

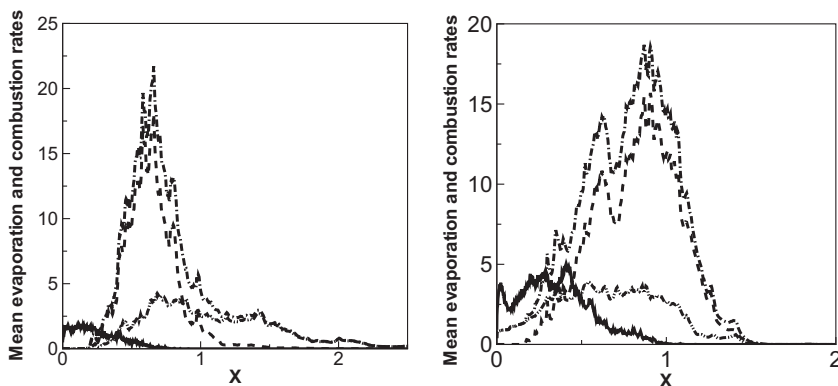


Fig. 5. Conditional mean evaporation and combustion rates for the lean (left) and rich (right) cases (—: evaporation rate; ---: total combustion rate; -·-·: premixed combustion rate; ···: diffusion combustion rate).

droplet evaporation. To examine this, the conditional mean scalar dissipation rates (CMSDR) evaluated over cross-sections at given x -positions with conditioning on mixture fraction are shown for the lean and rich cases in Fig. 7. As expected, closer to the nozzle exit, the values of scalar dissipation rate are higher due to spray evaporation, and the dissipation rates are generally higher for the rich case. It is noteworthy that the CMSDR shows multiple modes. In the lean case, a bimodal bell-shaped profile is observed at different axial locations. The rich case is similar, but has the minimum at a higher mixture fraction value and has an additional region of high dissipation rate at higher mixture fraction values. The reason for the multi-modal shape of the CMSDR is twofold. First, the complexity of the flow field with multiple recirculation regions causes the minimum at the lower mixture fraction value. Both outer and inner recirculation region bring burnt well mixed gases from the downstream region back to the nozzle. The mixture fraction of these gases corresponds therefore roughly to the global equivalence ratio of the considered case, which are $Z_{\text{global}} = 0.044$ for the lean case and $Z_{\text{global}} = 0.12$ for the rich case. This is evident in the mixture fraction distribution close to the nozzle for the lean case (figure not shown). The maximum at lower mixture fraction hence describes mixing between the hot gases in the outer recirculation and the outer injected air stream. The next maximum describes the main mixing region between the injected fuel and the surrounding air streams. The second reason for the multi-modal profiles is the effect of evaporation. This is especially clear for the rich case, where the third very rich peak is caused directly by evaporating droplets. These high values of scalar dissipation rate in the rich mixture due to evaporation have also been observed by Wandel et al. [13]. But also for the lower mixture fraction regions, the dissipation rates are strongly enhanced by evaporation, lead-

ing to substantially higher dissipation rates than in the regions of low mixture fraction where evaporation rates go to zero, as further discussed in the following section.

4.3. Conditional mean evaporation rate

In the conditional moment closure (CMC) method [14] or in the mixture fraction variance transport equation [15], modeling the unclosed correlation of scalar and evaporation source term is challenging and remains an open problem. To provide insight into this, the conditional mean evaporation rates (CMER) in mixture fraction space at different axial locations are shown in Fig. 8.

In both lean and rich cases, the CMER is negligibly small on the lean side compared with the rich side. Further from the nozzle exit, the evaporation rate becomes lower as expected. Although the CMER increases almost linearly with mixture fraction for the lean case, which is consistent with previous observations [14,15], this does not seem to be valid for the rich case. In the latter case, the CMER increases first, but then decreases, and the local maximum value depends on the axial location. This might suggest that the one droplet model (ODM) proposed in [15], which is the basis for the linear assumption for the CMER is limited to lean condition.

4.4. PDF of mixture fraction

In combustion modeling, a presumed β -function PDF is often used to describe the mixture fraction. Although this has been shown typically to be quite a good approximation for combustion of gaseous fuels [16,17], the β -function PDF may not such a good model in spray combustion, since mixture fraction is no longer a conserved scalar. In particular, the mixture fraction originates only through evaporation of liquid fuel, which appears

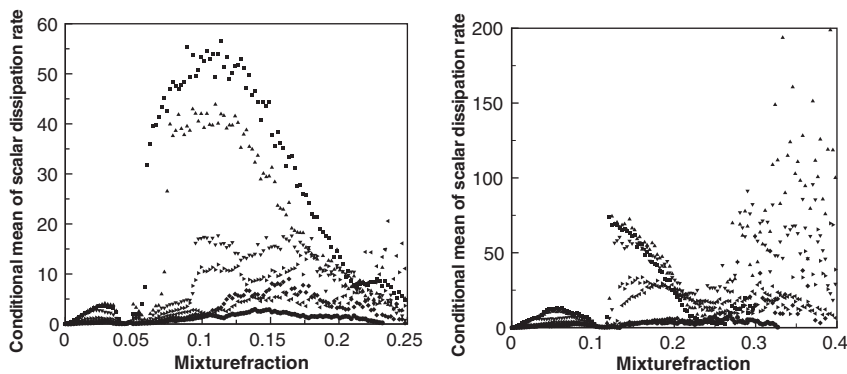


Fig. 7. Conditional mean scalar dissipation rate at different axial locations for the lean (left) and rich (right) cases (■ : $x = 0.15$; ▲ : $x = 0.20$; ▼ : $x = 0.30$; ► : $x = 0.40$; ◀ : $x = 0.50$; ◆ : $x = 0.70$; and • : $x = 0.80$).

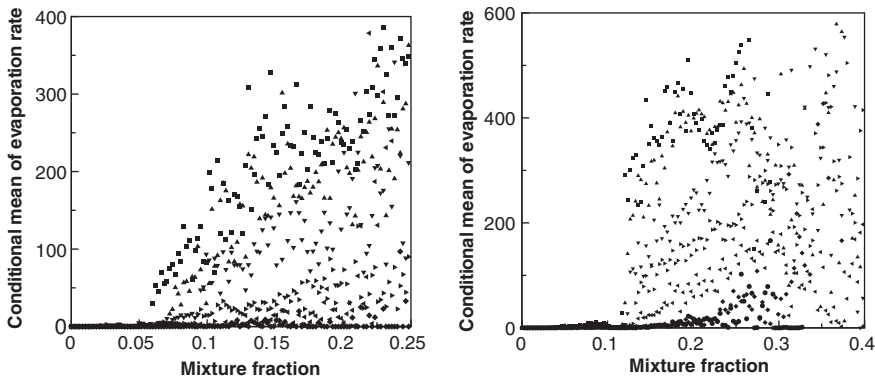


Fig. 8. Conditional mean evaporation rate at different axial locations for the lean (left) and rich (right) cases (■ : $x = 0.15$; ▲ : $x = 0.20$; ▼ : $x = 0.30$; ► : $x = 0.40$; ◄ : $x = 0.50$; ◆ : $x = 0.70$; and • : $x = 0.80$).

as a source term in the mixture fraction equation. This source term depends on mixture fraction and typically has a maximum at relatively low mixture fraction values. Because of this, the shapes of the mixture fraction PDF can be quite complex for liquid fuel combustion.

If one denotes the lean and rich limits of the range in which the mixture fraction Z varies as Z_L and Z_R , then in typical combustion processes, Z_L remains most often close to zero, because of small stoichiometric mixture fraction and a potential abundance of air. For spray combustion Z_R is typically substantially lower than unity. Pitsch [18] suggested in the context of flamelet modeling to introduce a transformed mixture fraction that always varies between zero and unity as

$$\zeta = \frac{Z - Z_L}{Z_R - Z_L}, \quad (3)$$

which is similar to the more recent suggestion of Ge and Gutheil [19] to formulate the β -function PDF such that it describes a scalar varying between a minimum and a maximum value. However, the main question is how to define these minimum and maximum values. Pitsch [18] used $Z_L = 0$ and suggested to use

$$Z_R = \langle Z \rangle + \alpha \sqrt{\langle Z^2 \rangle - \langle Z \rangle^2} \quad \text{with} \quad \alpha = 2, \quad (4)$$

where the brackets denote the averaging operator that defines the PDF, which will be tested here.

The PDFs of mixture fraction as well as the mean and variance are obtained from the simulation results over planes of given x . As shown in Fig. 9, the PDF of mixture fraction shows a strong peak at zero mixture fraction, an approximately equal distribution over a certain range, and a slight peak at the highest observed mixture fraction, which is approximately equal to the value of $Z_R = 0.058$ given by Eq. (4). Further downstream first the rich peak disappears at $x = 0.3$ and then the lean peak disappears at

$x = 0.6$. At the far downstream locations of $x = 3.0$ and beyond, the PDFs assume a more Gaussian shape.

The model approximates the PDFs quite well in the first and the last two positions. The delta peak at zero mixture fraction is also represented very accurately in the second position. However, the model still suggests a slight peak at the maximum mixture fraction value of $Z_R = 0.15$, which means that Eq. (4) slightly underpredicts the value of Z_R . The most notable difference occurs in the third position, where the shape of the PDF gradually changes into a Gaussian profile. Here again, the model for Z_R suggests a value that is too small. This is to be expected for strongly skewed distributions. It is interesting to note that in the ζ -space as tested here with $Z_L = 0$, the downstream PDFs move to very large values. The reason is that in these regions Z_R and Z_L are of the same order and the assumption that $Z_L = 0$ does not hold anymore. However, it can be observed that this does not compromise the model performance.

These results confirm that the presumed standard β -PDF needs to be modified for spray combustion modeling [14,19], and the model proposed by Ge and Gutheil [19] is a good choice.

5. Summary and conclusions

Analysis of *n*-heptane spray combustion in a three-dimensional swirl combustor has been conducted using two different DNS datasets, one is for a leaner case resembling lean direct injection combustion, and the other is for a rich case, which resembles the primary combustion region of a rich-burn/quick-quench/lean-burn combustor concept. The flame structure was investigated and shown to be complex, with regions of premixed and non-premixed combustion. It is observed that premixed flames contribute more than 70% to the total heat release rate, although premixed combustion

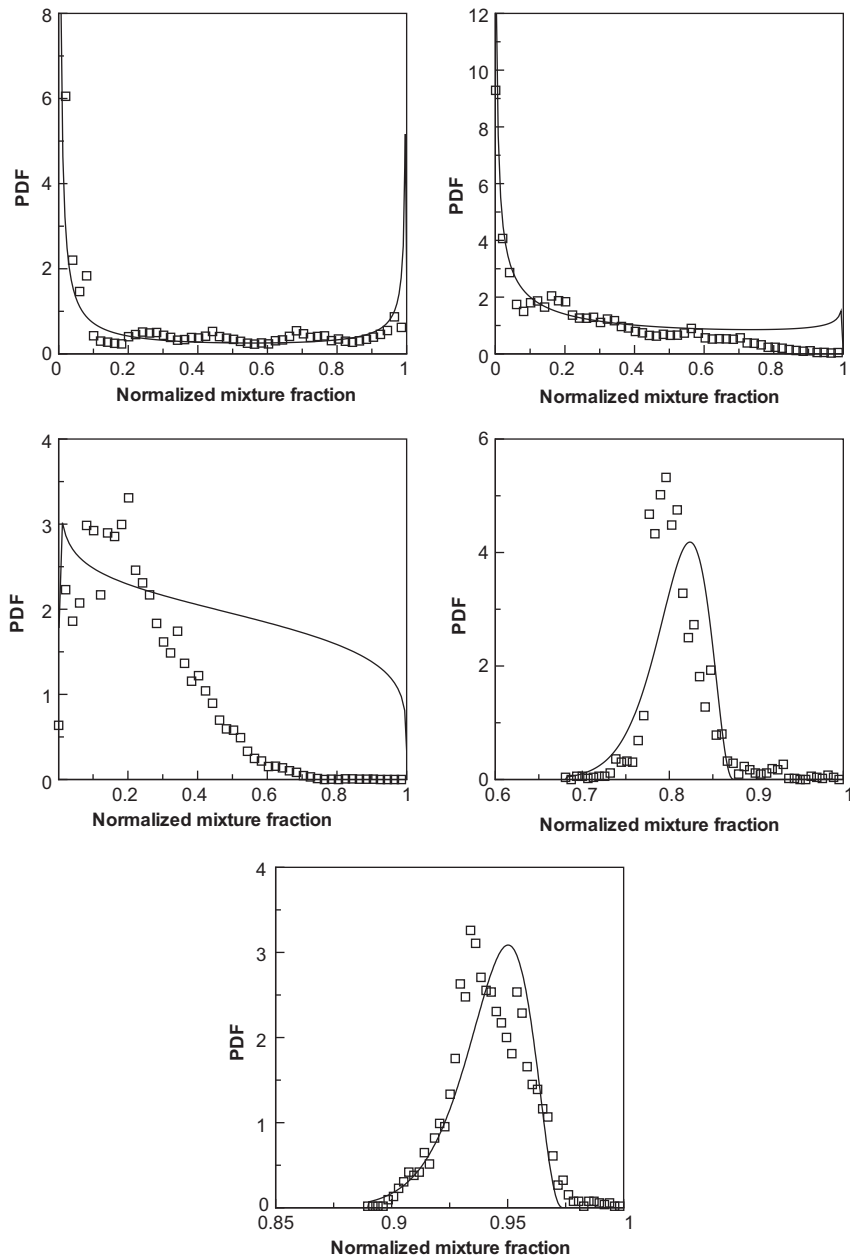


Fig. 9. PDFs of mixture fraction at different axial locations (top left: $x = 0.15, Z_R = 0.058$; top right: $x = 0.3, Z_R = 0.15$; middle left: $x = 0.6, Z_R = 0.15$; middle right: $x = 3.0, Z_R = 0.053$; bottom: $x = 5.0, Z_R = 0.051$) for the lean case.

regions cover a smaller volume than diffusion flames. Especially rich premixed combustion regions are shown to be important for flame stabilization. An accurate description of premixed and partially premixed combustion is therefore necessary to improve spray combustion modeling. The conditional mean scalar dissipation rate shows multiple modes. Most notably, there is an increase or even a peak in the very rich regions that is

caused by fuel evaporation. In both lean and rich cases, the conditional mean evaporation rate is negligibly small on the lean side compared with that on the rich side. Although the conditional mean evaporation rates increase almost linearly with mixture fraction in the lean case, the behavior for the rich case is more complex. To correctly describe the PDFs of mixture fraction in spray combustion modeling, the β -PDF formulated for

a transformed mixture fraction is found to be a reasonable model.

Acknowledgments

The authors are grateful to NASA's support of this project. K. Luo appreciates inspiring discussions and help from Professor Parviz Moin, Professor Luc Vervisch, Dr. Edward Knudsen, Dr. H. El-Asrag, Dr. Mehdi Raessi, and other colleagues at Stanford University. Computational resources at Texas Advanced Computing Center (TACC) are acknowledged. Fundings from the NSFC (50976098, 50736006) are also appreciated.

References

- [1] J. Réveillon, L. Vervisch, *J. Fluid Mech.* 537 (2005) 317–347.
- [2] P. Domingo, L. Vervisch, J. Réveillon, *Combust. Flame* 140 (2005) 172–195.
- [3] M. Nakamura, F. Akamatsu, R. Kurose, M. Katsuki, *Phys. Fluids* 17 (2005) 172–195.
- [4] C. Peraa, J. Réveillon, *Proc. Combust. Inst.* 31 (2007) 2283–2290.
- [5] E. Fernandez-Tarrazo, A.L. Sanchez, A. Linan, F.A. Williams, *Combust. Flame* 147 (2006) 32–38.
- [6] C.T. Crowe, S. Martin, Y. Tsuji, *Multiphase Flows with Droplets and Particles*, CRC Press, New York, USA, 1998.
- [7] R.S. Miller, K. Harstad, J. Bellan, *Int. J. Multiphase Flow* 24 (1998) 1025–1055.
- [8] K. Luo, O. Desjardins, H. Pitsch, in: *Annual Research Briefs*, Center for Turbulence Research, NASA Ames/Stanford University, 2008.
- [9] K. Luo, M. Pai, H. Pitsch, in: *Annual Research Briefs*, Center for Turbulence Research, NASA Ames/Stanford University, 2009.
- [10] K. Mahesh, G. Constantinescu, S. Apte, G. Iaccarino, F. Ham, P. Moin, *J. Appl. Mech.* 73 (2006) 374.
- [11] P. Moin, S. Apte, *AIAA J.* 44 (4) (2006) 698–708.
- [12] O. Desjardins, G. Blanquart, G. Balarac, H. Pitsch, *J. Comp. Phys.* 227 (2008) 7125–7159.
- [13] A.P. Wandel, N. Chakraborty, E. Mastorakos, *Proc. Combust. Inst.* 32 (2009) 2283–2290.
- [14] N.S.A. Smith, C.M. Cha, H. Pitsch, J.C. Oefelein, in: *Proceedings of the Summer Program*, Center for Turbulence Research, NASA Ames/Stanford University, 2000, pp. 207–218.
- [15] J. Reveillon, L. Vervisch, in: *Proceedings of the Summer Program*, Center for Turbulence Research, NASA Ames/Stanford University, 1998, pp. 25–38.
- [16] N. Peters, *Prog. Energy Combust. Sci.* 10 (1984) 319–339.
- [17] C.D. Pierce, P. Moin, *J. Fluid Mech.* 504 (2004) 73–97.
- [18] H. Pitsch, Modellierung der zündung und schadstoffbildung bei der dieselmotorischen verbrennung mit hilfe eines interaktiven flamelet-modells, Ph.D. Thesis, RWTH Aachen, 1998.
- [19] H.W. Ge, E. Gutheil, *Atomization Sprays* 16 (2006) 531–542.